# Bounds on the Error Variance when Estimating the Position of an Image

B. Moision[1]

*We illustrate Cramer–Rao lower bounds (CRLBs) on the root-mean-square (RMS) error in estimating the position of an image on a detector array. Several models of the image intensity distribution are treated. The case of Poisson arrivals and a Gaussian image profile, which was treated in [1], is extended to treat an unknown image mean and a skew-normal profile with unknown skew. We show the bounds are insensitive to knowledge of the mean while unknown skew can result in a loss of ≈1.5 dB. We show that a time-varying image profile, with pixel variance quadratic in the image mean, leads to a floor in the RMS error as a function of the mean.*

## I. Introduction

The high frequency of an optical communications link is both a boon and a curse to an optical system designer. High frequencies allow narrow beam widths that yield good power efficiency but require highly accurate pointing and tracking. This makes an accurate pointing system a critical component of a deep-space optical communications link. For example, a 1064-nm laser with a 30-cm aperture yields a far-field beam width of ≈3.56 $\mu$rad. A typical link budget requires a root-mean-square (RMS) pointing error of less than 1/10 of the beam width, in this case 0.356 $\mu$rad.

To achieve highly accurate pointing, a deep-space link may utilize an image of the Earth, with Earth imaging done in either the visible or infrared bands, see, e.g., [2,3]. An image of the Earth is received on a focal-plane array on the spacecraft with time-varying distortions that degrade estimation accuracy. In this article, we compute bounds on the performance of a spatial tracking algorithm that utilizes an image of the Earth. We extend results from [1] to treat a skew-Gaussian image, which is a more accurate depiction of an infrared image and model uncertainty in the image in terms of unknown image skew. We also extend the results of [4] to treat conditional Poisson statistics, which more accurately model a time-varying image profile, and relate the model from [4] to other models.

[1] Communications Architectures and Research Section.

The research described in this publication was carried out by the Jet Propulsion Laboratory, California Institute of Technology, under a contract with the National Aeronautics and Space Administration.

## II. Problem Definition

Let $I(\boldsymbol{\rho})$ be the normalized ($\int I(\boldsymbol{\rho}) = 1$) intensity distribution of an image incident on an $L$ detector array. The offset image with intensity distribution $I(\boldsymbol{\rho} - \boldsymbol{r})$ is received in the presence of noise. Given an observation of the noisy image, the receiver computes an estimate $\hat{\boldsymbol{r}}$ of the unknown offset $\boldsymbol{r} = (r_1, r_2)$, presumed to be a realization of a random process. In the following, we determine Cramer–Rao lower bounds (CRLBs) on the variance

$$\sigma_{\hat{\boldsymbol{r}}}^2 = \left\langle (\hat{\boldsymbol{r}} - \boldsymbol{r})^2 \right\rangle$$

of an unbiased estimate $\hat{\boldsymbol{r}}$.

The noise and image energy fields yield photoelectron counts over a given area that are random Poisson variates with mean proportional to the integrated energy over a slot time. Let $\lambda_s$ denote the total mean image photoelectrons and $A_i$ the aperture of the $i$th detector—a $2\delta \times 2\delta$ square centered at $(\rho_{i,1}, \rho_{i,2})$. Assume the mean noise photons per detector, $\lambda_n$, are constant over the array. Let

$$\begin{aligned} g_i(\boldsymbol{r}) &= \text{fraction of image captured by } i\text{th detector} \\ &= \int_{A_i} I(\boldsymbol{\rho} - \boldsymbol{r}) d\boldsymbol{\rho} \\ \lambda_i &= \text{mean photons detected by } i\text{th detector} \\ &= \lambda_s g_i(\boldsymbol{r}) + \lambda_n \\ k_i &= \text{photons detected by } i\text{th detector} \end{aligned}$$

The image is characterized by a collection of unknown parameters $\boldsymbol{\theta} = (\theta_1, \theta_2, \cdots)$. The unknown parameters always include the position, $\boldsymbol{\theta} = (r_1, r_2 \cdots)$, and may, in the more general case, include other parameters of the image that are unknown at the detector. Uncertainty in the estimation of these additional parameters will degrade the accuracy in estimation of $\boldsymbol{r}$. Let $\hat{\boldsymbol{\theta}} = [\hat{\boldsymbol{r}}_1, \hat{\boldsymbol{r}}_2, \cdots]$ be the estimate of $\boldsymbol{\theta}$.

The output of the $i$th detector is conditionally Poisson, with probability mass function

$$p(k_i | \boldsymbol{\theta}, \boldsymbol{\lambda}) = \frac{\lambda_i^{k_i} e^{-\lambda_i}}{(k_i)!}$$

where $\boldsymbol{\lambda} = (\lambda_1, \lambda_2, \cdots, \lambda_L)$. The detector outputs are assumed independent, so that the joint mass function of the array output $\boldsymbol{k} = (k_1, \cdots, k_L)$ is given by

$$p(\boldsymbol{k} | \boldsymbol{\theta}, \boldsymbol{\lambda}) = \prod_{i=1}^{L} \frac{\lambda_i^{k_i} e^{-\lambda_i}}{(k_i)!}$$

(a case of correlated observations is treated in Section VI.C). In the general case, due, for example, to albedo variations, $\boldsymbol{\lambda}$ may be the realization of a random process. Integrating over the joint density of $\boldsymbol{\lambda}$ yields

$$p(\boldsymbol{k}|\boldsymbol{\theta}) = \int p(\boldsymbol{k}|\boldsymbol{\theta}) p(\boldsymbol{\lambda}) d\boldsymbol{\lambda}$$

Let $\hat{\boldsymbol{r}}$ be an unbiased estimate of $\boldsymbol{r}$ and assume the joint density satisfies the regularity condition

$$\left\langle \frac{\partial \ln p(\boldsymbol{k}|\boldsymbol{\theta})}{\partial \boldsymbol{\theta}} \right\rangle = \mathbf{0} \;\; \forall \boldsymbol{r}$$

Then the estimate variance satisfies the CRLB, see, e.g., [5],

$$\sigma^2_{\hat{\boldsymbol{\theta}}_i} \geq \left[ I^{-1}(\boldsymbol{\theta}) \right]_{i,i}$$

where $I$ is the Fisher information matrix

$$\left[ I(\boldsymbol{\theta}) \right]_{i,j} = \left\langle \frac{\partial \ln p(\boldsymbol{k}|\boldsymbol{\theta})}{\partial \theta_i} \frac{\partial \ln p(\boldsymbol{k}|\boldsymbol{\theta})}{\partial \theta_j} \right\rangle$$

For example, consider the case where $\boldsymbol{\theta} = (r_1, r_2)$. Let

$$a = \frac{1}{\lambda_s} \left\langle \left( \frac{\partial \ln p}{\partial r_1} \right)^2 \right\rangle \tag{1}$$

$$b = \frac{1}{\lambda_s} \left\langle \left( \frac{\partial \ln p}{\partial r_2} \right)^2 \right\rangle \tag{2}$$

$$d = \frac{1}{\lambda_s} \left\langle \frac{\partial \ln p}{\partial r_1} \frac{\partial \ln p}{\partial r_2} \right\rangle \tag{3}$$

Then we have

$$I(\boldsymbol{k}) = \lambda_s \begin{bmatrix} a & d \\ d & b \end{bmatrix}$$

and

$$\sigma^2_{\hat{\boldsymbol{r}}|\boldsymbol{r}} = \left\langle (\hat{\boldsymbol{r}} - \boldsymbol{r})^2 | \boldsymbol{r} \right\rangle$$

$$\geq \frac{1}{\lambda_s} \frac{a+b}{ab - d^2} \tag{4}$$

Throughout we assume the image is entirely captured in the detector array so that $\sum_i g_i(\boldsymbol{r}) = 1$ and $\sum_i g_i'(r_1) = 0$. We also assume that the prior on $\boldsymbol{r}$ is uniform over the array. If the detector area were infinite and the prior on $\boldsymbol{r}$ were uniform, then any estimate would be invariant to a translation by an integer number of pixels, and it is sufficient to integrate over a single pixel area to obtain the mean-square error [1]:

$$\sigma^2_{\hat{\boldsymbol{r}}} = \frac{1}{4\delta^2}\int_{-\delta}^{\delta}\int_{-\delta}^{\delta}\sigma^2_{\hat{\boldsymbol{r}}|\boldsymbol{r}}d\boldsymbol{r}$$

We continue to make this simplifying assumption for a finite array. Substituting and factoring out the image mean yields

$$\sigma^2_{\hat{\boldsymbol{r}}} \geq \frac{1}{\lambda_s}G \tag{5}$$

where

$$G = \frac{1}{4\delta^2}\int_{-\delta}^{\delta}\int_{-\delta}^{\delta}\frac{a+b}{ab-d^2}d\boldsymbol{r}$$

In the following sections, we compute functions analogous to $G$ in Eq. (5) for different models of $I(\boldsymbol{\rho})$. Section IV treats the case where $I(\boldsymbol{\rho})$ is deterministic and known and arrivals are Poisson; subsections treat the cases where the mean and skewness are unknown. Section V treats the case of random means yielding negative-binomial arrivals, and Section VI treats the case of Gaussian arrivals with an unknown profile. First, in the following section, we present two models for the deterministic component of the brightness distribution.

## III. Models for the Intensity Distribution

In this section, we present two models for the deterministic component, or mean value, of an intensity distribution. The intensity distribution affects the results through the functions $g_i(\boldsymbol{r})$ and their derivatives $g_i'(\theta_i) = \partial g_i(\boldsymbol{r})/\partial\theta_i$. Results in later sections are stated in terms of $g_i(\boldsymbol{r}), g_i'(\theta_i)$, and may be extended to different intensity distribution models in a straightforward manner by substituting these functions.

Figure 1 illustrates a sample intensity distribution of Earth in the infrared. To obtain the distribution, near-Earth infrared data from the Atmospheric Infrared Sounder were extrapolated to a distance of 2 AU by filtering with aperture blurring and adding noise (background, shot, and sensor dark noise).[2] The distribution appears Gaussian with some skew. We will use both a normal and skew-normal distributions as models of the true distribution.

### A. Normal Intensity Distribution

Let $\phi(x;\sigma) = \left(1/\sqrt{2\pi\sigma^2}\right)e^{-x^2/(2\sigma^2)}$, a zero-mean normal density, and

$$I(\boldsymbol{\rho}) = \phi(\rho_1;\sigma)\phi(\rho_2;\sigma) \tag{6}$$

a bivariate normal distribution. Let $\xi_{i,1} = \rho_{i,1} - r_1$ and $\xi_{i,2} = \rho_{i,2} - r_2$, the shifted center of the $i$th pixel. Then

[2] S. Piazzolla, *Reconstructing Earth Emission from AIRS*, (internal document), Jet Propulsion Laboratory, Pasadena, California, 2005.

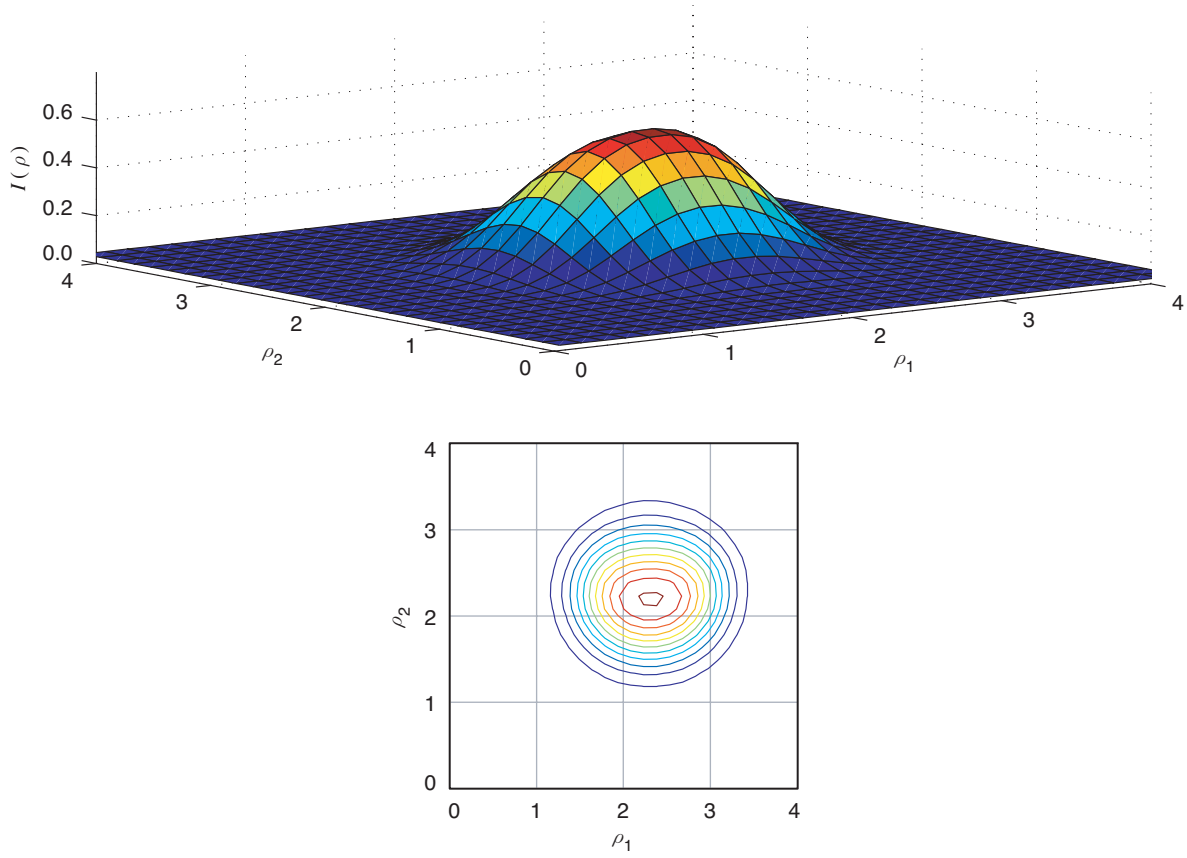


**Fig. 1. Example of an intensity distribution extrapolated from AIRS data,** $\delta = 0.5$**.**

$$g_i(\boldsymbol{r}) = \int_{A_i - \boldsymbol{r}} I(\boldsymbol{\rho}) d\boldsymbol{\rho}$$

$$= \int_{\xi_{i,1}-\delta}^{\xi_{i,1}+\delta} \phi(\rho_1;\sigma) d\rho_1 \int_{\xi_{i,2}-\delta}^{\xi_{i,2}+\delta} \phi(\rho_2;\sigma) d\rho_2$$

with partial derivative

$$g_i'(r_1) = \frac{\partial g_i(\boldsymbol{r})}{\partial r_1}$$

$$= \frac{1}{2}\left(\operatorname{erfc}\left(\frac{1}{\sqrt{2\sigma^2}}(\xi_{i,2}-\delta)\right) - \operatorname{erfc}\left(\frac{1}{\sqrt{2\sigma^2}}(\xi_{i,2}+\delta)\right)\right)$$

$$\times \frac{1}{\sqrt{2\pi\sigma^2}}\left(\exp\left(-\frac{1}{2\sigma^2}(\xi_{i,1}-\delta)^2\right) - \exp\left(-\frac{1}{2\sigma^2}(\xi_{i,1}+\delta)^2\right)\right)$$

where

$$\operatorname{erfc}(x) = \frac{2}{\sqrt{\pi}} \int_x^\infty e^{-t^2} dt$$

### B. Skew-Normal Intensity Distribution

In order to capture the skewness of the observed data, we also consider a skew-normal distribution, see, e.g., [6],

$$I(\boldsymbol{\rho}) = 4\phi(\rho_1;\sigma_1)\Phi(\alpha_1\rho_1)\phi(\rho_1;\sigma_2)\Phi(\alpha_2\rho_2) \tag{7}$$

where $\Phi(x) = (1/\sqrt{2\pi}\,)\int_{-\infty}^{x} e^{-t^2/2}dt = \int_{-\infty}^{x}\phi(t,1)dt$, the cumulative distribution function of a zero-mean unit-variance normal density. This scaled version of the bivariate normal density allows some skew by means of the parameters $\alpha_1, \alpha_2$ and reduces to the normal when $\alpha_1 = \alpha_2 = 0$. Figure 2 illustrates an example of a skew-normal distribution. Let

$$\Psi(x, y, \sigma, \delta) = 2\int_{x}^{y}\phi(\rho;\sigma)\Phi(\delta\rho)d\rho \tag{8}$$

Then

$$g_i(\boldsymbol{r}) = \Psi(\xi_{i,1}-\delta, \xi_{i,1}+\delta, \sigma_1, \alpha_1)\Psi(\xi_{i,2}-\delta, \xi_{i,2}+\delta, \sigma_2, \alpha_2) \tag{9}$$

$$\begin{aligned} g_i'(r_1) &= 2\Psi(\xi_{i,2}-\delta, \xi_{i,2}+\delta, \sigma_2, \alpha_2) \\ &\quad\times\big(\phi(\xi_{i,1}-\delta;\sigma_1)\Phi\big(\alpha_1(\xi_{i,1}-\delta)\big) - \phi(\xi_{i,1}+\delta;\sigma_1)\Phi\big(\alpha_1(\xi_{i,1}+\delta)\big)\big) \end{aligned}$$

$$\begin{aligned} g_i'(\alpha_1) &= \Psi(\xi_{i,2}-\delta, \xi_{i,2}+\delta, \sigma_2, \alpha_2)\frac{\sigma_1^2}{\pi(1+\sigma_1^2\alpha_1^2)} \\ &\quad\times\left(\exp\left(\frac{-(\xi_{i,1}-\delta)^2(1+\sigma_1^2\alpha_1^2)}{2\sigma_1^2}\right) - \exp\left(\frac{-(\xi_{i,1}+\delta)^2(1+\sigma_1^2\alpha_1^2)}{2\sigma_1^2}\right)\right) \end{aligned}$$

In numerical results, we evaluate Eq. (8) by numerical integration. The marginal of Eq. (7) has mean

$$\sqrt{\frac{2}{\pi}}\frac{\alpha_1\sigma_1^2}{(1+\alpha_1^2\sigma_1^2)^{1/2}}$$

and variance

$$\sigma_1^2\left(1-\frac{2}{\pi}\frac{\sigma_1^2\alpha_1^2}{1+\sigma_1^2\alpha_1^2}\right)$$

The mean is irrelevant in our comparisons; however, in comparisons with the normal intensity, we choose $\sigma_1, \sigma_2$ such that the variances of the marginals are equal to the variances of the marginals of the normal.

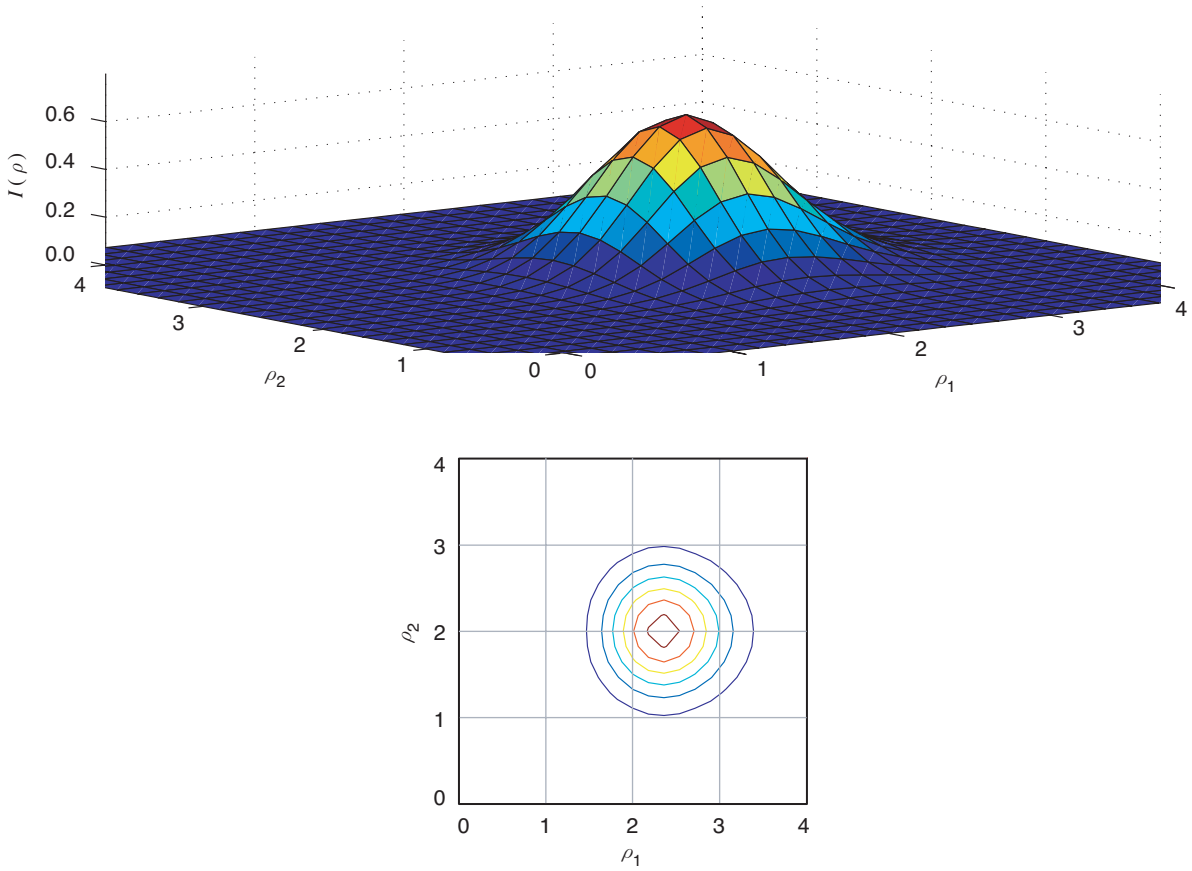


**Fig. 2. A skew-normal distribution with** $\delta = 0.5$, $\alpha_1 = 0$, $\alpha_2 = 2$, $\sigma_1 = 0.5$, $\sigma_2 = 0.64$.

## IV. Known Intensity Distribution, Poisson Arrivals

Suppose $I(\boldsymbol{\rho})$ and $\lambda_s$ are known to the detector, so that $\boldsymbol{\theta} = \boldsymbol{r}$. This could be the case, for example, with a known beacon, and serves as a limiting case when other parameters are unknown. Then

$$p(\boldsymbol{k}|\boldsymbol{r}) = \prod_{i=1}^{L} \frac{\lambda_i^{k_i} e^{-\lambda_i}}{(k_i)!}$$

The terms $a, b, d$, defined by Eqs. (1) through (3), reduce to

$$a = \sum_{i=1}^{L} \frac{1}{\tilde{\lambda}_i} \big(g_i'(r_1)\big)^2 \tag{10}$$

$$b = \sum_{i=1}^{L} \frac{1}{\tilde{\lambda}_i} \big(g_i'(r_2)\big)^2 \tag{11}$$

$$d = \sum_{i=1}^{L} \frac{1}{\tilde{\lambda}_i} g_i'(r_1) g_i'(r_2) \tag{12}$$

where $\tilde{\lambda}_i = \lambda_i/\lambda_s = g_i(\boldsymbol{r}) + \lambda_n/\lambda_s$. This yields

$$\sigma_{\hat{\boldsymbol{r}}}^2 \geq \frac{1}{\lambda_s} G_n(\delta, \sigma, \lambda_n/\lambda_s) \tag{13}$$

$$G_n(\delta, \sigma, \lambda_n/\lambda_s) = \frac{1}{4\delta^2} \int_{-\delta}^{\delta} \int_{-\delta}^{\delta} \frac{a+b}{ab-d^2} d\boldsymbol{r} \tag{14}$$

We see the error variance is inversely linear in the image mean for a fixed $\lambda_s/\lambda_n$, and the normalized error $\sigma_{\hat{\boldsymbol{r}}}^2 \lambda_s$ depends only on the ratio $\lambda_s/\lambda_n$, as illustrated in [1].

Figure 3 reproduces a result from [1], illustrating the normalized 2-D RMS error $\sigma_{\hat{\boldsymbol{r}}}\sqrt{\lambda_s}/\sigma$ as a function of the pixel-to-image-size ratio $2\delta/\sigma$ for $I(\boldsymbol{\rho})$ normal, Eq. (6). Figure 4 illustrates the RMS error $\sigma_{\hat{\boldsymbol{r}}}$ in units of pixel lengths (i.e., $\delta$ is set to 0.5) as a function of the image mean for varying noise means. For example, we see that if we desire an RMS error of less than a tenth of a pixel, we require an image mean of at least 66 photons per image. In Fig. 4, $\sigma = \delta = 0.5$, since, as shown in Fig. 4, a pixel-width-to-image standard deviation of approximately 2 is optimum over a wide range of image and noise pairs. In the limit of small background, the multiplier goes to $G_n(0.5, 0.5, 0) \approx 0.67$.

### A. Gaussian Intensity, Unknown Image Mean

In practice, it may be necessary to estimate the image mean, which will be varying due to variations in the Earth albedo. Let $\boldsymbol{\theta} = [r_1, r_2, \lambda_s]$ and

$$c = \frac{1}{\lambda_s} \left\langle \frac{\partial \ln p}{\partial \lambda_s}^2 \right\rangle = \frac{1}{\lambda_s^2} \sum_{i=1}^{L} \frac{g_i(\boldsymbol{r})^2}{\tilde{\lambda}_i}$$

$$e = \frac{1}{\lambda_s} \left\langle \frac{\partial \ln p}{\partial r_1} \frac{\partial \ln p}{\partial \lambda_s} \right\rangle = \frac{1}{\lambda_s} \sum_{i=1}^{L} \frac{g_i(\boldsymbol{r}) g_i'(r_1)}{\tilde{\lambda}_i}$$

$$f = \frac{1}{\lambda_s} \left\langle \frac{\partial \ln p}{\partial r_2} \frac{\partial \ln p}{\partial \lambda_s} \right\rangle = \frac{1}{\lambda_s} \sum_{i=1}^{L} \frac{g_i(\boldsymbol{r}) g_i'(r_2)}{\tilde{\lambda}_i}$$

It follows that

$$\sigma_{\hat{\boldsymbol{r}}}^2 \geq \frac{1}{\lambda_s} G_{n,2}(\delta, \sigma, \lambda_n/\lambda_s)$$

where

$$G_{n,2}(\delta, \sigma, \lambda_n/\lambda_s) = \frac{1}{4\delta^2} \int_{-\delta}^{\delta} \int_{-\delta}^{\delta} \frac{a+b-\frac{1}{c}(e^2+f^2)}{ab-d^2+\frac{1}{c}(2def-e^2b-af^2)} d\boldsymbol{r}$$

$\tilde{\lambda}_i = \lambda_i/\lambda_s$ and $a, b, d$ are given by Eqs. (10) through (12). In the absence of noise, $\lambda_n = 0$, we have $e = f = 0$, and the error variance reduces to Eq. (4). Figure 5 illustrates $G_{n,2}/G_n$ in decibels, the relative gain in $\lambda_s$ to achieve the same bound on $\sigma_{\hat{\boldsymbol{r}}}^2$, as a function of $\lambda_s/\lambda_n$. With a Gaussian intensity profile, we see an error variance close to Eq. (4) (less than uncertainty in numerical evaluation of the integrals). Hence, the position estimate is not sensitive to knowledge of the image mean.

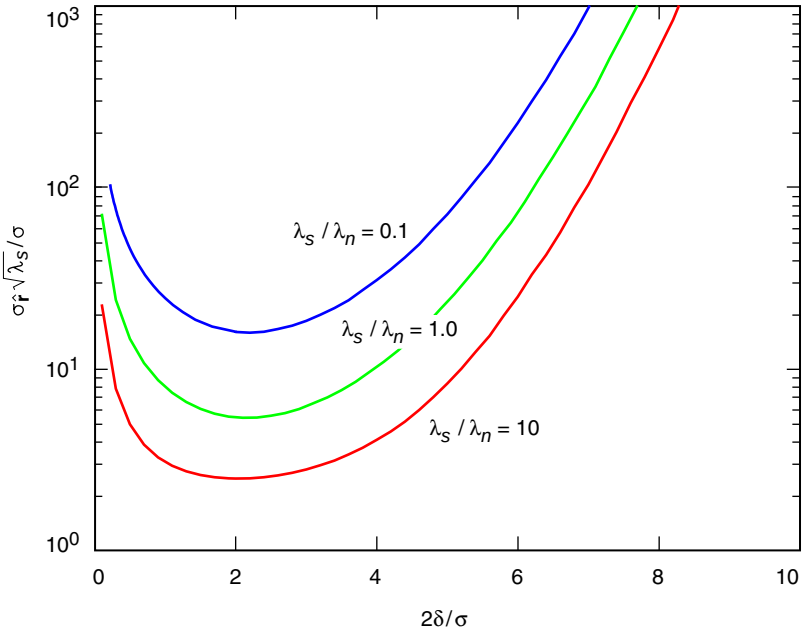


**Fig. 3. Lower bound on normalized RMS error in position estimate as a function of pixel size on image variance.**

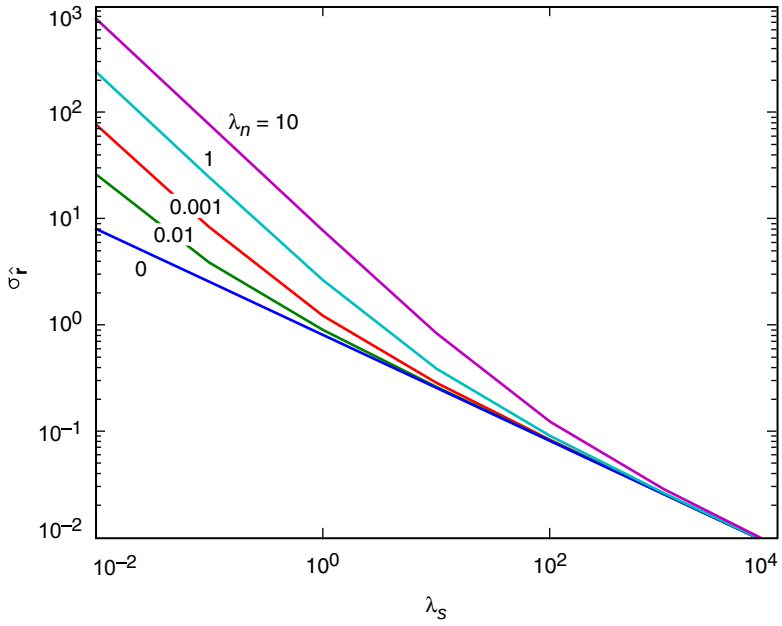


**Fig. 4. Lower bound on RMS error in position estimate.**

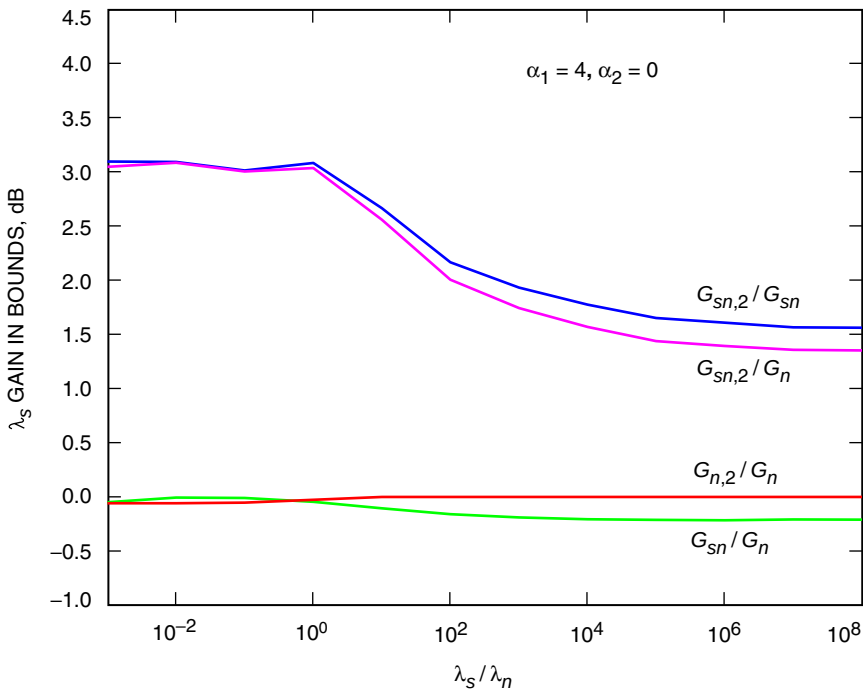


**Fig. 5. Relative difference in bounds (dB). All skew-normal distributions have $\alpha_1 = 4$, $\alpha_2 = 0$.**

### B. Skew-Normal Intensity, Unknown Skew

We may model uncertainty in the image distribution by assuming the distribution is skew-normal with an unknown skew. Here we examine the impact of not knowing one of the skewness parameters. Let $\boldsymbol{\theta} = [r_1, r_2, \alpha_1]$ and

$$c = \frac{1}{\lambda_s} \left\langle \frac{\partial \ln p}{\partial \alpha_1}^2 \right\rangle = \sum_{i=1}^{L} \frac{1}{\tilde{\lambda}_i} \big(g_i'(\alpha_1)\big)^2$$

$$e = \frac{1}{\lambda_s} \left\langle \frac{\partial \ln p}{\partial r_1} \frac{\partial \ln p}{\partial \alpha_1} \right\rangle = \sum_{i=1}^{L} \frac{1}{\tilde{\lambda}_i} g_i'(r_1) g_i'(\alpha_1)$$

$$f = \frac{1}{\lambda_s} \left\langle \frac{\partial \ln p}{\partial r_2} \frac{\partial \ln p}{\partial \alpha_1} \right\rangle = \sum_{i=1}^{L} \frac{1}{\tilde{\lambda}_i} g_i'(r_2) g_i'(\alpha_1)$$

It follows that

$$\sigma_{\hat{\boldsymbol{r}}}^2 \geq \frac{1}{\lambda_s} G_{sn,2}(\delta, \sigma, \lambda_n/\lambda_s) \tag{15}$$

where

$$G_{sn,2}(\delta,\sigma,\lambda_n/\lambda_s) = \frac{1}{4\delta^2}\int_{-\delta}^{\delta}\int_{-\delta}^{\delta}\frac{a+b-\frac{1}{c}(e^2+f^2)}{ab-d^2+\frac{1}{c}(2def-e^2b-af^2)}d\boldsymbol{r}$$

$\tilde{\lambda}_i = \lambda_i/\lambda_s$, $a, b, d$ are given by Eqs. (10) through (12), and $g_i(\boldsymbol{r})$ is given by Eq. (9). Similar to the normal, let $G_{sn} = G_{sn,2}|_{e=f=0}$, the scaling factor of a skew-normal with known skew. We set the pixel length to $\delta = 0.5$ and set $\sigma_1, \sigma_2$ such that the standard deviations of the marginals of the intensity are equal to $\delta$. Figure 5 illustrates the ratio of scale factors for $G_n, G_{sn}$ and $G_{sn,2}$. The ratio yields the difference in $\lambda_s$ required to achieve the same RMS error as a function of $\lambda_s/\lambda_n$. When $\lambda_s \gg \lambda_n$, we see a loss of 1.5 dB between the skew-normal with unknown skew and the normal (and a similar loss between the skew-normal with known and unknown skew). When the skew is known, we see only a small difference between the normal and skew-normal (some skew actually reduces the RMS error bound).

## V. $I(\boldsymbol{\rho})$ Random, Negative-Binomial Arrivals

In the previous sections, we assumed the image density was deterministic, with possibly unknown parameters. In practice, the image intensity is time-varying. A time-varying image intensity may be modeled as a random process, and a realization of this yields pixel means $\lambda_i$ that are random variables. In this section, we treat this case by modeling the integrated intensity of the optical receivers as random variates with a Gamma-distribution [7, Section 4.5]

$$p(\lambda_i) = \frac{\lambda_i^{M-1}e^{-M\lambda_i/\langle\lambda_i\rangle}}{\Gamma(M)}\left(\frac{M}{\langle\lambda_i\rangle}\right)^M$$

where, for a fully developed speckle field, $M$ is the speckle count, which is known at the receiver, and

$$\langle\lambda_i\rangle = \lambda_s\int_{A_i-\boldsymbol{r}} I(\boldsymbol{\rho})d\boldsymbol{\rho} = \lambda_s g_i(\boldsymbol{r})$$

where $I(\boldsymbol{\rho})$ is the mean intensity, also presumed known, and we have set $\lambda_n = 0$, to simplify discussion. The $k_i$ have a negative-binomial distribution

$$\begin{aligned} p(k_i) &= \int_0^\infty p(k_i|\lambda_i)p(\lambda_i)d\lambda_i \\ &= \binom{k_i+M-1}{k_i}\frac{\langle\lambda_i\rangle^{k_i}M^M}{\left(M+\langle\lambda_i\rangle\right)^{k_i+M}} \end{aligned}$$

with mean and variance

$$\langle k_i\rangle = \langle\lambda_i\rangle$$

$$\sigma_{k_i}^2 = \langle\lambda_i\rangle + \frac{\langle\lambda_i\rangle^2}{M}$$

Here the variance of the photon counts is quadratic in the received signal mean. We will see that this quadratic growth in the uncertainty restricts the rate of decrease of the RMS error. Let $\boldsymbol{\theta} = [r_1, r_2]$. The elements of the Fisher information matrix for this case are given by

$$a = \frac{1}{\lambda_s}\left\langle \left(\frac{\partial \ln p}{\partial r_1}\right)^2 \right\rangle = \sum_i \frac{g_i'(r_1)^2}{g_i(\boldsymbol{r})}\left(\frac{M}{\lambda_s g_i(\boldsymbol{r}) + M}\right)$$

$$b = \frac{1}{\lambda_s}\left\langle \left(\frac{\partial \ln p}{\partial r_2}\right)^2 \right\rangle = \sum_i \frac{g_i'(r_2)^2}{g_i(\boldsymbol{r})}\left(\frac{M}{\lambda_s g_i(\boldsymbol{r}) + M}\right)$$

$$d = \frac{1}{\lambda_s}\left\langle \frac{\partial \ln p}{\partial r_1}\frac{\partial \ln p}{\partial r_2} \right\rangle = \sum_i \frac{g_i'(r_1) g_i'(r_2)}{g_i(\boldsymbol{r})}\left(\frac{M}{\lambda_s g_i(\boldsymbol{r}) + M}\right)$$

and the variance bound is given by Eqs. (13) and (14). Figure 6 illustrates the RMS error as a function of the signal mean parameterized by $M$. The image density is normal with $\sigma = 0.5$; the pixel width is one: $\delta = 0.5$; and the background is zero: $\lambda_n = 0$. The results approach the Poisson for $M \gg \lambda_s$, as the negative-binomial approaches the Poisson for large $M$. In the limit of large $\lambda_s$, the bound on $\sigma^2_{\hat{\boldsymbol{r}}}$ approaches the limit

$$\frac{1}{M}\frac{1}{\delta^2}\int_{-\delta}^{\delta}\int_{-\delta}^{\delta} \frac{\sum_i \left(g_i'(r_1)/g_i(\boldsymbol{r})\right)^2 + \left(g_i'(r_2)/g_i(\boldsymbol{r})\right)^2}{\sum_i \left(g_i'(r_1)/g_i(\boldsymbol{r})\right)^2 \sum_j \left(g_j'(r_2)/g_j(\boldsymbol{r})\right)^2 - \left(\sum_i \left(g_i'(r_1) g_i'(r_2)\right)/g_i(\boldsymbol{r})^2\right)^2} dr_1 dr_2$$

hence the error variance cannot be decreased arbitrarily by increasing the signal mean. This type of behavior was observed with a Gaussian approximation to the conditional Poisson model in [4], which we address in the following section.

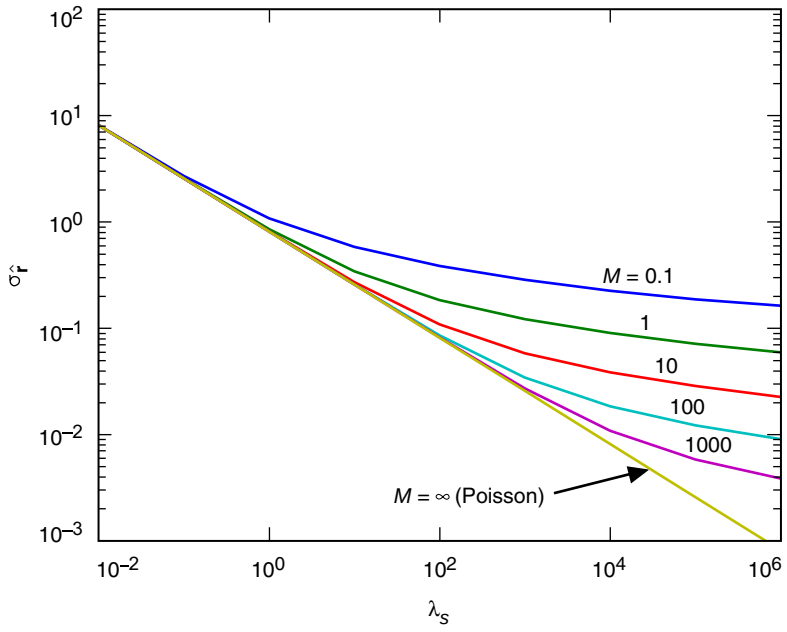


**Fig. 6. Lower bound on RMS error in position estimate, negative-binomial arrivals.**

## VI. $I(\boldsymbol{\rho})$ Random, Gaussian Arrivals

In the prior sections, we presumed either the intensity profile was known, was known with unknown parameters, or was random with a known mean. In [4] the estimate of the intensity profile is modeled as a random offset of the true profile. Here we revisit the approach from [4], relating it to other models, extending the results to a correlated noise case, and illustrating their connection with the Poisson in the limit. In this section, we presume the noise background is zero: $\lambda_n = 0$.

Suppose the image intensity distribution is given by

$$I(\boldsymbol{\rho}) = \hat{I}(\boldsymbol{\rho}) + \tilde{I}(\boldsymbol{\rho})$$

where $\hat{I}(\boldsymbol{\rho})$ is a deterministic, estimated intensity distribution, and $\tilde{I}(\boldsymbol{\rho})$ represents an error in that estimate, modeled as a zero-mean Gaussian process with autocorrelation $R(\boldsymbol{\rho}; \boldsymbol{\rho}')$. To simplify analysis, let the observed photon counts be equal to their mean,

$$\begin{aligned} k_i = \lambda_i &= \lambda_s g_i(\boldsymbol{r}) \\ &= \lambda_s \int_{A_i - \boldsymbol{r}} I(\boldsymbol{\rho}) d\boldsymbol{\rho} \\ &= \lambda_s \big( \hat{g}_i(\boldsymbol{r}) + \tilde{g}_i(\boldsymbol{r}) \big) \end{aligned}$$

where

$$\hat{g}_i(\boldsymbol{r}) = \int_{A_i - \boldsymbol{r}} \hat{I}(\boldsymbol{\rho}) d\boldsymbol{\rho}$$

$$\tilde{g}_i(\boldsymbol{r}) = \int_{A_i - \boldsymbol{r}} \tilde{I}(\boldsymbol{\rho}) d\boldsymbol{\rho}$$

The photon counts are Gaussian random variables with mean

$$\begin{aligned} \langle \lambda_i \rangle &= \lambda_s \int_{A_i - \boldsymbol{r}} \hat{I}(\boldsymbol{\rho}) d\boldsymbol{\rho} \\ &= \lambda_s \hat{g}_i(\boldsymbol{r}) \end{aligned}$$

and covariance

$$\begin{aligned} \boldsymbol{C}_{i,j} &= \big\langle \big( \lambda_i - \langle \lambda_i \rangle \big) \big( \lambda_j - \langle \lambda_j \rangle \big) \big\rangle \\ &= \lambda_s^2 \big\langle \tilde{g}_i(\boldsymbol{r}) \tilde{g}_j(\boldsymbol{r}) \big\rangle \\ &= \lambda_s^2 \int_{A_i - \boldsymbol{r}} \int_{A_j - \boldsymbol{r}} R(\boldsymbol{\rho}; \boldsymbol{\rho}') d\boldsymbol{\rho} d\boldsymbol{\rho}' \end{aligned}$$

which is characterized by the autocorrelation of the Gaussian noise process. The joint density of the photon counts is

$$p(\boldsymbol{\lambda}|\boldsymbol{r}) = \frac{1}{\sqrt{(2\pi)^L|\boldsymbol{C}|}} \exp\left(-\frac{1}{2}(\boldsymbol{\lambda} - \langle\boldsymbol{\lambda}\rangle)\boldsymbol{C}^{-1}(\boldsymbol{\lambda} - \langle\boldsymbol{\lambda}\rangle)^T\right)$$

and the elements of the scaled Fisher information matrix are given by [5, Eq. (3.31)][3]

$$a = \frac{1}{\lambda_s}\left\langle\left(\frac{\partial \ln p}{\partial r_1}\right)^2\right\rangle = \sum_{i,j}\lambda_s\hat{g}_i'(r_1)\hat{g}_j'(r_1)\boldsymbol{C}_{ij}^{-1} - \frac{1}{2\lambda_s}\left(\frac{\partial \boldsymbol{C}_{ij}}{\partial r_1}\right)\left(\frac{\partial \boldsymbol{C}_{ij}^{-1}}{\partial r_1}\right) \tag{16}$$

$$b = \frac{1}{\lambda_s}\left\langle\left(\frac{\partial \ln p}{\partial r_2}\right)^2\right\rangle = \sum_{i,j}\lambda_s\hat{g}_i'(r_2)\hat{g}_j'(r_2)\boldsymbol{C}_{ij}^{-1} - \frac{1}{2\lambda_s}\left(\frac{\partial \boldsymbol{C}_{ij}}{\partial r_2}\right)\left(\frac{\partial \boldsymbol{C}_{ij}^{-1}}{\partial r_2}\right) \tag{17}$$

$$d = \frac{1}{\lambda_s}\left\langle\left(\frac{\partial \ln p}{\partial r_1}\right)\left(\frac{\partial \ln p}{\partial r_2}\right)\right\rangle = \sum_{i,j}\lambda_s\hat{g}_i'(r_1)\hat{g}_j'(r_2)\boldsymbol{C}_{ij}^{-1} - \frac{1}{2\lambda_s}\left(\frac{\partial \boldsymbol{C}_{ij}}{\partial r_1}\right)\left(\frac{\partial \boldsymbol{C}_{ij}^{-1}}{\partial r_2}\right) \tag{18}$$

so that the CRLB is

$$\sigma_{\hat{\boldsymbol{r}}}^2 \geq \frac{1}{4\delta^2\lambda_s}\int_{-\delta}^{\delta}\int_{-\delta}^{\delta}\frac{a+b}{ab-d^2}d\boldsymbol{r} \tag{19}$$

We consider here several examples for the covariance of the additive noise process and the implications on the error variance.

### A. Uncorrelated Offset with Variance Proportional to Mean

Let

$$R(\boldsymbol{\rho}, \boldsymbol{\rho}') = \frac{\gamma^2}{A\lambda_s}\Delta(\boldsymbol{\rho} - \boldsymbol{\rho}')$$

where $A$ is the area of a pixel, $\Delta(\cdot)$ is the Dirac delta function, and $\gamma^2/(A\lambda_s)$ is the variance of $\tilde{I}$, which is inversely proportional to the signal power. Then

$$C_{ij} = \gamma^2\lambda_s\Delta_{ij}$$

(here $\Delta$ is the Kronecker delta function). Here, as with the case of Poisson arrivals with a deterministic profile, the variance is a linear function of the mean (note that the noise process is given by $\lambda_s\tilde{I}(\boldsymbol{\rho})$) and

$$\sigma_{\hat{\boldsymbol{r}}}^2 \geq \frac{\gamma^2}{\lambda_s}G_g$$

[3] Note that the second term in the corresponding sums [4, Eqs. (17a) through (17c)] are off by a factor of $-1/2$.

where

$$G_g = \frac{1}{4\delta^2}\int_{-\delta}^{\delta}\int_{-\delta}^{\delta}\frac{\sum_i \hat{g}_i'(r_1)^2 + \hat{g}_i'(r_2)^2}{\left(\sum_i \hat{g}_i'(r_1)^2\right)\left(\sum_j \hat{g}_j'(r_2)^2\right) - \left(\sum_i \hat{g}_i'(r_1)\hat{g}_i'(r_2)\right)^2}dr_1 dr_2 \tag{20}$$

Here the error increases linearly with the mean of the noise process and decreases linearly with the image mean. In this case, one can drive the error variance to be as small as desired by increasing the image mean. With $\hat{I}(\boldsymbol{\rho})$ Gaussian, given by Eq. (6), $\delta = 0.5$, and $\sigma = 0.5$, numerical integration, including enough terms in the sums to have negligible contributions from the tails of the intensity distribution, yields $G_g \approx 6.2$.

### B. Variance Proportional to Square of the Mean

Let

$$R(\boldsymbol{\rho};\boldsymbol{\rho}') = \frac{\gamma^2}{A}\Delta(\boldsymbol{\rho}-\boldsymbol{\rho}')$$

where $A$ is the area of a pixel. Then

$$C_{ij} = \gamma^2\lambda_s^2\Delta_{ij}$$

and

$$\sigma_{\hat{\boldsymbol{r}}}^2 \geq \gamma^2 G_g$$

with $G_g$ given by Eq. (20). Here the noise mean, as with the negative-binomial model, is quadratic in the signal mean. This could arise, for example, in the presence of Albedo variations, where increasing the image mean by increasing the integration time leads to increases in the variance. As with the negative-binomial model, we observe a floor in the error variance beyond which increasing the signal mean does not decrease the variance.

### C. Correlated Noise Power

Suppose the distribution noise arises from Albedo variation. It is realistic for the noise from these elements to be correlated due to filtering of the signal by the receive aperture. We'll consider a simple case where adjacent pixels are correlated with variance quadratic in the signal mean:

$$C_{ij} = \begin{cases} \gamma^2\lambda_s^2, & i = j \\ \dfrac{\gamma^2\lambda_s^2}{2}, & \text{pixel } i \text{ adjacent to pixel } j \\ 0, & \text{otherwise} \end{cases}$$

With $\hat{I}(\rho)$ Gaussian, given by Eq. (6), $\delta = 0.5$, and $\sigma = 0.5$, numerical evaluation of Eq. (19) yields

$$\sigma_{\hat{\boldsymbol{r}}}^2 \gtrapprox \gamma^2(13.5)$$

In this case, the noise correlation leads to an increase in the error variance by a factor of $13.5/6.2 = 2.18$.

### D. Gaussian as Approximation to Poisson

When the photon count is sufficiently large, Poisson arrivals may be modeled as Gaussian. In this regime, the Gaussian approximation will agree with the Poisson. To see this, set the Gaussian variance equal to the mean

$$C_{ij} = \langle \lambda_i \rangle \Delta_{ij} = \lambda_s \hat{g}_i(\boldsymbol{r}) \Delta_{ij}$$

Substitution into Eq. (16) yields

$$\frac{1}{\lambda_s} \left\langle \left( \frac{\partial \ln p}{\partial r_1} \right)^2 \right\rangle = \sum_i \frac{\hat{g}_i'(r_1)^2}{\hat{g}_i(r_1)} \left( 1 + \frac{1}{2\lambda_s g_i(\boldsymbol{r})} \right) \tag{21}$$

and we obtain similar multipliers for Eqs. (17) and (18). We see that Eq. (21) reduces to the Poisson case, Eq. (10), for large $\lambda_s$ (when $\lambda_n = 0$, as was assumed throughout this section).

## VII. Conclusions

We have placed a number of models of distortions in an image under a common framework, allowing comparisons of the impact of the uncertainties on the variance in the image position estimate. We propose using a skew-Gaussian model for an Earth image to capture asymmetries in the image intensity. As noted in [4], if the variance of the photon counts is quadratic in the mean photon rate, then the error variance cannot be reduced below a certain threshold.

# References


[1] K. Winick, "Cramer–Rao Lower Bound on the Performance of Charge-Coupled-Device Optical Position Estimators," *Journal of the Optical Society of America*, vol. 3, pp. 1809–1815, November 1986.

[2] H. Hemmati, Y. Chen, S. Lee, and G. Ortiz, "Earth-Image Tracking in the IR for Deep Space Optical Communications," *Digest of the LEOS Summer Topical Meetings*, pp. 27–28, July 2005.

[3] A. Biswas, S. Piazolla, G. Peterson, G. G. Ortiz, and H. Hemmati, "The Long-Wave Infrared Earth Image as a Pointing Reference for Deep-Space Optical Communications," *The Interplanetary Network Progress Report*, vol. 42-167, Jet Propulsion Laboratory, Pasadena, California, pp. 1–29, November 15, 2006. http://ipnpr/progress_report/42-167/167D.pdf

[4] C.-C. Chen, "Effect of Earth Albedo Variation on the Performance of a Spatial Acquisition Subsystem Aboard a Planetary Spacecraft," *The Telecommunications and Data Acquisition Progress Report 42-95, July–September 1988*, Jet Propulsion Laboratory, Pasadena, California, pp. 202–211, November 15, 1988. http://ipnpr/progress_report/42-95/95T.PDF

[5] S. M. Kay, *Fundamentals of Statistical Signal Processing: Estimation Theory*, Upper Saddle River, New Jersey: Prentice Hall, 1993.

[6] A. K. Gupta, G. Gonzalez-Farias, and J. A. Dominguez-Molina, "A Multivariate Skew Normal Distribution," *Journal of Multivariate Analysis*, vol. 89, pp. 181–190, 2004.

[7] G. R. Osche, *Optical Detection Theory*, Wiley Series in Pure and Applied Optics, Hoboken, New Jersey: Wiley, 2002.